RSC Advances

PAPER

View Article Online
View Journal | View Issue

Cite this: *RSC Adv.*, 2023, **13**, 8586

Biocompatible polymers with tunable mechanical properties and conductive functionality on two-photon 3D printing†

Lijun Men,[a] Kemin Wang,[ab] Ningning Hu,[a] Fule Wang,[c] Yucheng Deng,[a] Wenjun Zhang*[ad] and Ruixue Yin *[c]

Two-photon polymerization (TPP)-based 3D printing technology utilizes the two-photon absorption process of near-infrared radiation, enabling the fabrication of micro- and nano-scale three-dimensional structures with extremely high resolution. It has been widely applied in scientific fields closely related to living organisms, such as tissue engineering, drug delivery, and biosensors. Nevertheless, the existing photoresist materials have poor mechanical tunability and are hardly able to be doped with functional materials, resulting in constraints on the preparation of functional devices with micro–nano structures. In this paper, TPP printable polymer formulas with good mechanical tunability, high resolution, strong functional scalability, and excellent biocompatibility are proposed, by using the synergistic effects of a hydroxyl group-containing photocurable resin prepolymer, UV acrylate monomer, long-chain hydrophilic crosslinking monomer and photo-initiator. This can ensure the printability and help to improve the flexibility of the printed polymer, thereby solving the problem the photosensitive materials suitable for two-photon 3D printing in previous research had in balancing the formability and flexibility. The results of nanoindenter analysis showed that the Young's modulus of the printed structure can be adjusted between 0.3 GPa and 1.43 GPa, realizing mechanical tunability. Also, complex structures, such as micro-scaffold structures and high aspect ratio hollow microneedles were printed to explore the structural stability as well as the feasibility of biodevice application. Meanwhile, the proposed polymer formula can be functionalized to be conductive by doping with functional nanomaterial MXene. Finally, the biocompatibility of the proposed polymer formula was studied by culturing with human normal lung epithelial cells. The results indicated a good potential for biodevice applications.

Received 23rd November 2022
Accepted 6th March 2023

DOI: 10.1039/d2ra07464h

rsc.li/rsc-advances

1. Introduction

Two-photon laser direct writing technology is a high-efficiency and high-precision three-dimensional structure preparation technology.[1] Compared with the traditional laser direct writing technology, TPP has the advantages of high resolution, simple process, adjustable parameters, and a wide selection of candidate materials in the fabrication of complex three-dimensional micro–nano structures.[1–3,6] TPP technology greatly reduces the difficulty of fabricating complex 3D structures, enabling truly rapid 3D prototyping. As a powerful 3D designable nano/micro prototyping technology, two-photon polymerization (TPP) nanolithography has become a key technology for fabricating 3D nano/microstructures for biological applications including cell engineering,[7–9] tissue engineering,[10–12] drug delivery,[13–16] biological microfluidic devices,[17–19] biological microrobots,[20–23] and biomedical devices. Currently, SU-8 resists, IP series resists, polyethylene glycol-based hydrogel materials, protein biomolecules, and hybrid inorganic–organic materials (HIOMs) have been used to construct 3D nano/micro-structures by TPP 3D printing.[24–26] However, the existing photoresist materials have poor mechanical tunability and are hardly able to be doped with functional materials, resulting in constraints on the preparation of functional bio-devices with micro–nano structures.[4,5] Meanwhile, most micro–nano devices are aiming to biomedical applications. Therefore, for TPP printed polymer structures, they must have biocompatibility suitable for cell attachment and proliferation, and be able to support the mechanical stability of cell tissues. Till now, there is still a lack of biocompatible photoresists with specific tunable mechanical properties based on TPP printing. At the same time, how to quickly optimize the laser parameters matched with a certain

[a]*Shanghai University, School of Mechanical and Electrical Engineering, No. 99, Shangda Road, Baoshan District, Shanghai, China*

[b]*Mingche Biotechnology Co., Ltd, No. 18, Jinfang Road, Suzhou, China*

[c]*East China University of Science and Technology, School of Mechanical and Power Engineering, No. 130, Meilong Road, Xuhui District, Shanghai, China. E-mail: yinruixue@ecust.edu.cn*

[d]*Division of Biomedical Engineering, University of Saskatchewan, Saskatoon, SK S7N 5A9, Canada. E-mail: wjz485@mail.usask.ca*

† Electronic supplementary information (ESI) available. See DOI: https://doi.org/10.1039/d2ra07464h

photoresist material to obtain high-quality devices is a challenging task.

In addition, to develop 3D functional structures, photoresist materials should be able to mix with various functional nanomaterials.[27,28] However, most of the functional materials that can be doped, such as conductive carbon nanotubes (CNTs), are toxic to a certain extent, and their biocompatibility is not very good. Therefore, the reasonable selection of biocompatible functional materials has a profound impact on the fabrication of functional micro–nano devices. MXene has been investigated as a more biocompatible conductive nanomaterial for bio-device development. Rastin *et al.* developed a conductive cell-loaded bioink for 3D printing, consisting of Ti_3C_2 MXene nanosheets dispersed in hyaluronic acid hydrogel, to fabricate wearable sensing devices at the millimeter scale.[29]

Although researchers have prepared functional structures through photolithography, the effective use of functional composite resin materials strongly depends on the weight percentage and dispersion quality of functional nanomaterials in composite materials. It is still of great challenges in preparing functional composite resin materials with high doping concentration of functional nanomaterials. Wei Xiong *et al.* proposed a method to incorporate well-aligned multi-walled carbon nanotubes into 2D/3D polymer structures *via* TPP printing technology, which significantly improved the electrical conductivity and mechanical strength of the photoresist. And a TPP-compatible, homogenous MTA composite resins with high MWNT concentrations (up to 0.2 wt%) has been developed by Wei Xiong's group.[4,5] However, to the best of our knowledge, there are no reports on resin materials containing MXene nanomaterials that can be used for two-photon 3D printing. Therefore, in order to give full play to the potential of functional materials, it is of great significance to develop TPP-adapted resin formulations that can be doped with high-concentration conductive MXene for the preparation of three-dimensional micro–nano integrated functional devices.

This paper proposed a biocompatible polymers-based photoresist formula with tunable mechanical properties and functionalities, and demonstrated the feasibility to fabricate complex structures with high resolution, such as nanowire structures, hollow microneedles with high aspect ratios, microspiral robots, and micro-logo structures. It helps to improve the flexibility of printed structures, thereby solving the problem that the photosensitive materials suitable for two-photon 3D printing in previous research are difficult to balance formability and flexibility. At the same time, the conductive functionality of the photoresist can be achieved by adding high concentration of Mxene, different from existed photoresists that cannot be doped with Mxene due to too large viscosity. The mechanical properties of printed micro–nano structures were well analyzed by a nano-indenter. Functional composite materials with electrical conductivity were obtained by adding high concentration of 0.2 wt% Mxene into the formula. The biocompatibility of the proposed material was investigated by culturing with human normal lung epithelial cells (BEAS-2B).

2. Materials and methods

2.1 Materials

BisGMA, epoxy methacrylate, was supplied by Sartomer, France. SR348OP, ethoxylated bisphenol A dimethacrylate, was provided by Sartomer, France. PEG600DMA, polyethylene glycol dimethacrylate, was provided by Sartomer, France. IC819, bisphenylphosphine oxide, was provided by Sigma Aldrich, Germany. MXene, $Ti_3C_2T_x$, provided by China Neocene Technology Company. BEAS-2B, human lung epithelial cells, provided by American type culture collection(ATCC). PBS, Phosphate Buffered Saline, supplied by Cytiva. DMEM, dulbecco's modified eagle medium, provided by Gibco. DAPI, cell viability and cytotoxicity assay reagents, provided by Beyotime.

2.2 Resin formulation

In this study, the as-prepared material containing photosensitizer, photoinitiator, and cross-linker for processing was defined as photoresist. Our formula is to mix 30 wt% of BisGMA and 70 wt% ofSR348OP, then add 50 wt% or 100 wt% of PEG600DMA to them respectively, and then fully stir the three to obtain a composite resin material. The chemical structures of the materials used above are shown in Fig. 1a. IC819 was used as the photoinitiator, and 2 wt% IC819 photoinitiator was added to all the above resin formulations. The proportions of each formula are shown in Table 1. In order to prepare a functional material formula, we mixed MXene ($Ti_3C_2T_x$) into the formula, and used a shaker to make it evenly mixed so that functional materials could be prepared. Finally, the resin material formulation is stored in an environment below 4 °C.

2.3 TPP setup

In this study, the TPP setup, named Photonic Professional (GT) system, was supplied by Nanoscribe company, Germany. GT

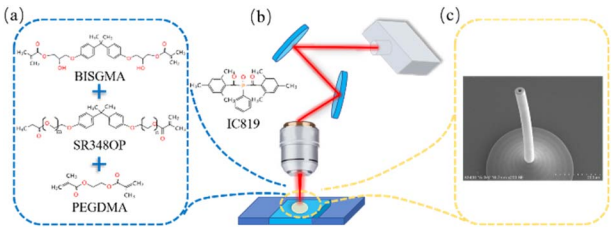

Fig. 1 (a) Chemical structure of the main components of photoresist. (b) Schematic diagram of TPP technique. (c) Oblique view of SEM image for 3D hollow microneedle.

Table 1 Main components of photoresist

	BisGMA	SR348OP	PEG600DMA	MXENE	IC819
0	29 wt%	71 wt%	0 wt%	0	2 wt%
1	20 wt%	46.7 wt%	33.3 wt%	0	2 wt%
2	15 wt%	35 wt%	50 wt%	0	2 wt%
3	20 wt%	46.7 wt%	33.3 wt%	0.2 wt%	2 wt%

system is designed to produce 2D, 2.5D, and 3D polymer structures with feature sizes ranging from sub-micron to millimeters using direct laser writing. The excitation parameters of the system are as follows: the central laser wavelength is 780 nm, the repetition frequency is 80 MHz, and the pulse width is 100 fs. The structures printed in this paper are mainly used in the DILL configuration of the GT system, in which the objective lens will be directly immersed into the photoresist. And since the DILL configuration is a reverse manufacturing process, the photoresist acts as both a photosensitive and immersion medium. Therefore, the maximum height of the structure is not limited, and structures with a height of less than 2 mm can be manufactured. Fig. 1b is a schematic diagram of the fabrication of microstructures using GT. In the fabrication process, the photoresist is dropped on the substrate, and the laser intensity is controlled by an attenuator. The focus of the laser is on the *XY* plane by Galvo for high-speed two-dimensional scanning, and the *Z*-axis direction is controlled by the movement of the piezo stage. Through the above preparation process, the three-dimensional micro–nano device shown in Fig. 1c can be obtained as an example.

2.4 Fabrication of complicated micro-structures

In this paper, the influence of laser parameters on the thickness of nanowire structures was investigated by preparing nanowire structures corresponding to different laser parameters. Meanwhile, in order to explore the printability of complex structures, specific structures have been fabricated, including a high-aspect-ratio hollow microneedle with a height of 1500 μm, a helical robot structure with a length of 120 μm and a width of 40 μm, and the logo of Shanghai University with a diameter of 200 μm. We also prepared a scaffold structure with a height of 120 μm and a length and width of 42 μm, and analyzed the stability of the structure through SEM characterization and error analysis of the structure. In order to explore the mechanical properties of the material formulation, a 20 μm × 20 μm × 12 μm bulk structure was prepared as a sample for nanoindentation test in this study.

2.5 Characterization

Scanning electron microscopy (SEM, JSM-7500F) was used to microscopically characterize the TPP fabricated structures. For mechanical tests, we performed nanoindentation experiments using a nanoindenter (UNHT^3, Anton Paar) provided by Anton Paar. In the nanoindentation experiments we used a diamond indenter and set a constant force of 0.1 mN to ensure nonlinear deformation of the polymer sample, and finally we can obtain the displacement load curve of the material to determine the Young's modulus. We used the ST2253 multifunctional digital four-probe tester to test the resistivity of the polymer containing the conductive functional material Mxene, so as to derive the conductivity of the polymer.

2.6 Cell culture and *in vitro* cytotoxicity test

We used human normal lung epithelial cells (BEAS-2B, ATCC) to perform biocompatibility experiments and cultured the cells using DMEM medium at a temperature of 37 °C and a carbon dioxide concentration of 5%. Before the biocompatibility test, we first sterilized the printed grid structures of the four formulations under an UV lamp for 2 h and then soaked them in normal saline (PBS) for 20 minutes. Aseptic treatment is followed by seeding of cells on top of the polymer structure. We first seeded primary human normal lung epithelial cells (BEAS-2B) on glass slides with two-dimensional polymers (four meshes with a size of 220 μm s^{-1} × 220 μm s^{-1} × 32 μm s^{-1}) with daily media exchange. After one or three days of culture, cells were washed with PBS buffer for 15 min at room temperature, and then stained with DAPI for 30 minutes. Using a Zeiss 20× lens, microscopic images were taken and the exposed glass surface around the grid was used as a negative control.

3. Results and discussion

3.1 Parameters of TPP fabrication

Lateral Spatial Resolution (LSR) is the width of the thinnest nanowires that can bemanufactured under a specific light intensity.[30] LSR has an significant influence on the precision of TPP micro machining.[7] Therefore, we investigated the LSR of photoresist formulations containing 0 wt% PEGDMA, 33 wt% PEGDMA and 50 wt% PEGDMA, respectively. The SEM images and related line width data were shown in Fig. 2 and 3, respectively.

Fig. 2a shows the SEM images with laser power from 15.5 mW to 40 mW at a laser scanning speed of 15 μm s^{-1} for the formula with PEGDMA content of 33 wt%. We observe that with the decrease of laser power, the line width decreases progressively, and the laser power corresponding to the minimal line width can reach 20 mW. In order to deeply study the relationship between the linewidth laser scanning speed, we set the laser power to 25 mW, 30 mW, and 35 mW respectively, and

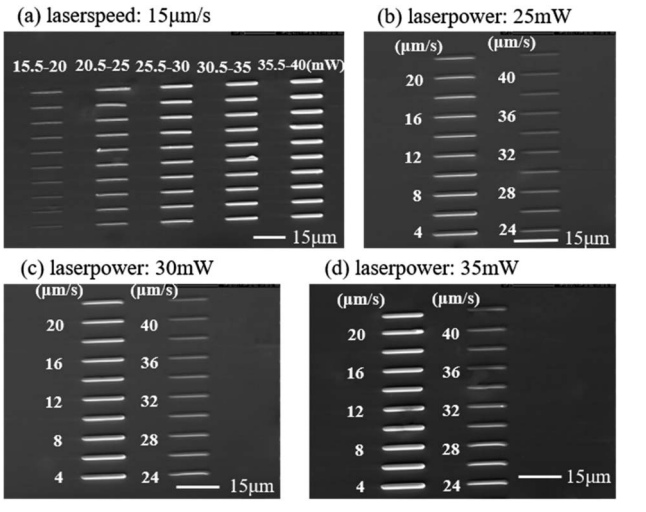

Fig. 2 (a) SEM images of nanowire arrays fabricated at a constant scanning velocity of 15 μm s^{-1} with the laser power ranging from 15.5 to 40 mW. (b)–(d) Top view of the scanning velocity increased from 4 to 40 μm s^{-1} with the laser power of 25 mW, 30 mW and 35 mW, respectively.

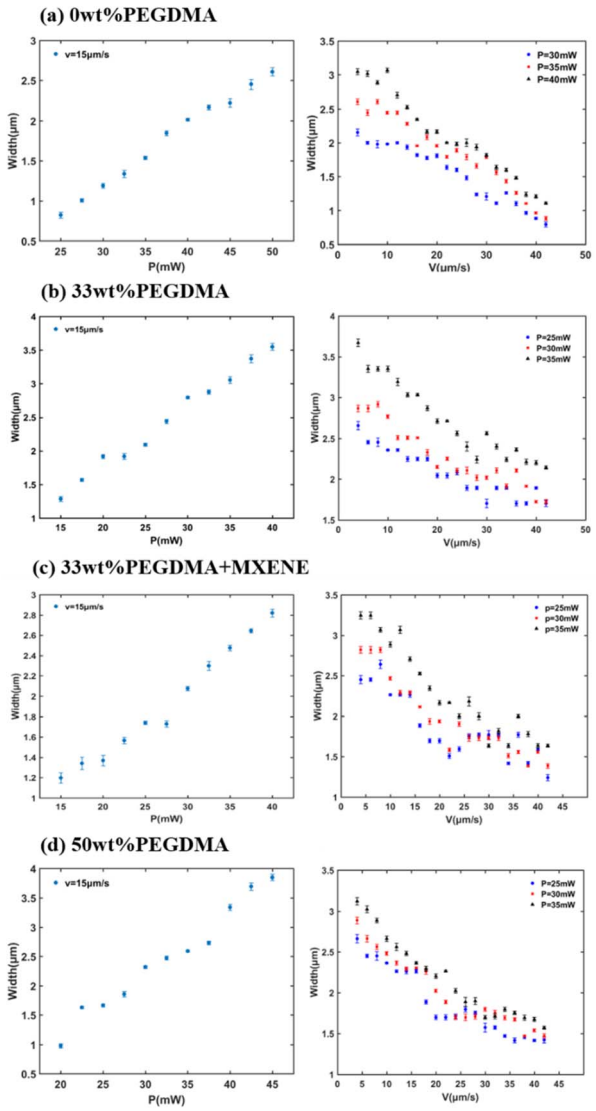

Fig. 3 Corresponding dependence of the line width on the scanning velocity for three kinds of as-prepared photoresist at different laser power. (a) Control with 0 wt% PEG600DMA, 29 wt% BisGMA and 71 wt% SR348OP. (b) Photoresist with 33.3 wt% PEG600DMA, 20 wt% BisGMA and 46.7 wt% SR348OP. (c) Photoresist with 33.3 wt% PEG600DMA, 20 wt% BisGMA, 46.7 wt% SR348OP and 0.1 wt%MXENE. (d) Photoresist with 50 wt% PEG600DMA, 15 wt% BisGMA and 35 wt% SR348OP.

make the laser scanning speed increase in steps of 2 μm s^{-1} under each power. Fig. 2b–d shows the nanowire arrays with the laser scanning speed increasing from 4 μm s^{-1} to 40 μm s^{-1} under different laser powers. It can be seen that with the increase of the scanning speed, the line width tends to decrease; and when the scanning speed remains unchanged, the line width also increases gradually with the increase of the laser power. For the three other photoresist formulations mentioned above, we carried out the above experiments and obtained the same results.

Fig. 3 is a quantitative comparison chart of the results from Fig. 2, which shows the variation of the width of the nanowires prepared with four different formulas as the laser power and laser speed change. Fig. 3 shows that after adding PEG600DMA, the line width has little effect, but the laser power range is considerably expanded. When the content of PEGDMA is 0 wt%, the lowest value of laser power is 25 mW, and the highest value reaches 60 mW, but when the content of PEGDMA is 33 wt% and 50 wt%, the lowest value of laser power can reach 15 mW, and the highest value can reach 75 mW. On the right-hand panels of Fig. 3a–d, it can be seen that when the laser power is constant, the faster the laser speed, the finer the fabricated nanowires. Based on the images to the left in Fig. 3a–d, when the laser speed is constant, the smaller the laser power, the finer the prepared nanowires. From the above results, it can be seen that when using the two-photon printer to fabricate 3D micro–nano devices, in order to improve the accuracy, the scanning speed of the laser should be increased as much as possible and the laser power should be reduced.

In order to compare the mechanical stability of the polymer, a self-supporting scaffold with a height of 120 μm and a length and width of 42 μm was manufactured.[31] The thickness of the horizontal bars was set to 1.5 μm and the distance between each bar was set to 8 μm. Its scanning electron microscope image is shown in Fig. 4a–d. The laser intensity required for the scaffold fabricated from the four photoresist formulas was 35 mW, and the scanning speed was 2000 μm s^{-1}. During the preparation of the three-dimensional scaffold structure, it is not difficult to find that the lateral characteristic width of the horizontal bar of the scaffold decreases with the increase of PEG600DMA content. By comparing the lateral characteristic widths of the horizontal rods of the scaffold structure prepared by the four materials, it can be seen that when the content of PEG600DMA is 50 wt%, the horizontal characteristic width of the horizontal strips can reach a minimum of 3.04 μm, and the accuracy can reach 0.01. At the same time, as the content of PEG600DMA increases from 0 wt% to 50 wt%, the lateral feature width of the horizontal rods of the scaffold will decrease from 3.5 μm to 3.04 μm. Fig. 4e is the data corresponding to the average area of the nine grids in the top view of the scaffold structures prepared with four different materials, and the area corresponding to each grid is extracted by the software Image-j. The areas of the grids in the view on the four formulas are 92.2 $μm^2$, 96.3 $μm^2$,

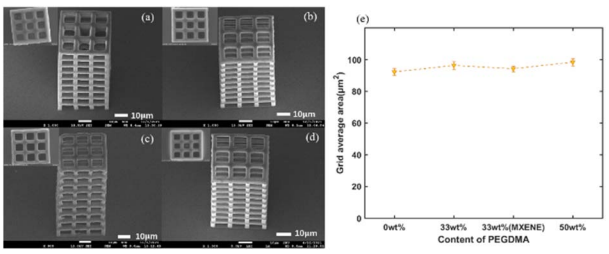

Fig. 4 (a–d) SEM images of the freestanding scaffold (sample tilt of 45°) with different PEGDMA content, and the upper left corner of each image corresponds to the top view of the current scaffold. (a) 0 wt% PEG600DMA; (b) 33.3 wt% PEG600DMA; (c) 50 wt% PEG600DMA; (d) 33.3 wt% PEG600DMA and 0.1 wt% MXENE. (e) Average area of grids in top view of scaffolds prepared with four formulas.

98.4 μm^2, and 94.2 μm^2, respectively. The above results show that after the addition of PEG600DMA, the lateral printing accuracy of the scaffold structure is improved, and the scaffold structure with high mechanical stability can still be fabricated with the addition of MXene.

3.2 Fabrication of complicated 3D structures

A series of complex structures (see Fig. 5) have been prepared to further explore the manufacturing ability of the proposed photoresist. Fig. 5a and b shows the SEM images of a high-aspect-ratio microneedle. The height of the actual printed microneedle is 1480 μm, the outer diameter is 42 μm, and the inner diameter is 12 μm, and the error with the actual microneedle structure is only 0.01. The surface morphology of the microneedle is smooth, which is highly adapted to our application in the biological domain. And till now, there has never been a hollow-core microneedle structure with an aspect ratio of 38.9 reported in literature, which has achieved a breakthrough in process manufacturing to a certain extent. Fig. 5c is the logo of Shanghai University with a diameter of 200 μm. The laser intensity used in the manufacturing process is 25 mW and the scanning speed is 3000 μm s^{-1}. Fig. 5d shows the morphological characterization of the helical robot structure with a length of 120 μm and a width of 40 μm prepared when the content of PEGDMA is 33 wt%. From the logo of Shanghai University in Fig. 5c and the micro-spiral robot in Fig. 5d, it can be seen that our improved photoresist can prepare micro–nano devices with complex and variable structures.

3.3 Mechanical properties and long-term stability

In this study, a nano-indenter was used to perform indentation tests on the 3D structure of each formula to explore the mechanical properties of the materials. In all experiments, the maximum load was set to a force of 0.1 mN in order to ensure the nonlinear deformation of the structure. From the

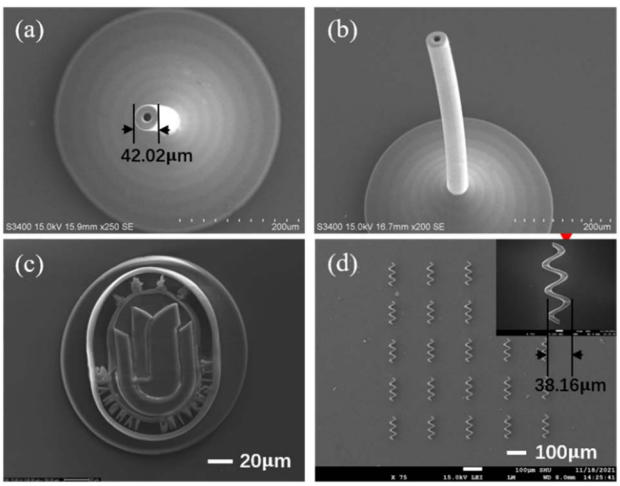

Fig. 5 SEM images of (a) top view of 3D hollow microneedle. (b) Oblique view of 3D hollow microneedle. (c) Top view of Shanghai University logo. (d) Top view of Helix Robot Array.

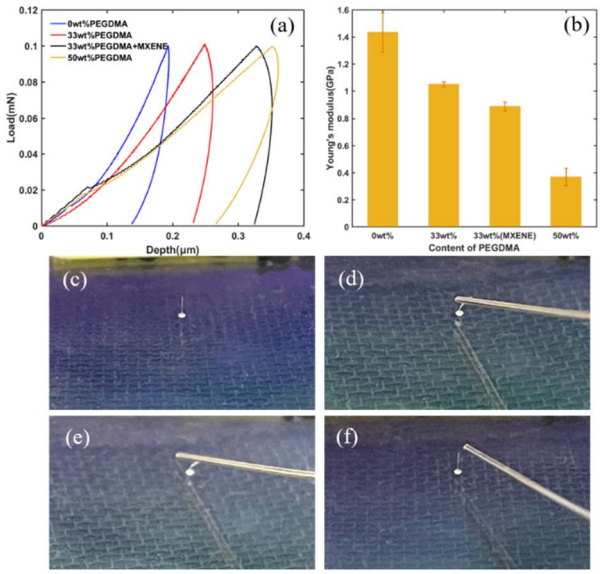

Fig. 6 (a) Displacement-loading curves of structures prepared with different contents of PEG600DMA. (b) Young's modulus bar chart of structures prepared with different contents of PEG600DMA. (c–f) Deformation of the hollow microneedle by manual pressing.

displacement load curve (Fig. 6a), it can be found that when the formula does not contain PEG600DMA, the deformation of the sample structure is the smallest, and the Young's modulus at this time is 1.4 GPa, indicating that the material itself has a relatively hard and crispy. On the contrary, with the increase of PEG600DMA content, the deformation amount of the structure also increases, indicating that the material itself is becoming softer and tougher. And when the PEG600DMA content is 33 wt%, the Young's modulus of the sample can still be maintained at about 1.05 GPa. Fig. 6b shows the Young's modulus of the four materials. It can be seen that with the increase of PEGDMA content, the Young's modulus of the material gradually decreases. At the same time, the Young's modulus of the formulation with the conductive material MXENE can also reach 0.8 GPa.

The above nanoindentation experimental results show that the materials provided in this study can achieve mechanically tunable properties under the conditions of satisfying printability and structural stability. In order to further determine the mechanical flexibility of the material, we manually pressed the hollow microneedle structure repeatedly, and finally found that the microneedle could always return to its original shape after multiple pressings. Fig. 6 c–f shows the operation of my pressing experiment described above. Experiments show that the improved material formula has strong flexibility. It can be seen from the above results that our material formulas are softer and more flexible than the BisSR[31] proposed by Boris Buchroithner *et al.* At the same time, by adjusting the content of PEGDMA, the mechanical properties of our materials have been improved in terms of flexibility, and the tunability of mechanical properties has been achieved.

To test the long-term stability of the mechanical properties of the microneedles, this study conducted another manual

pressing experiment on the microneedle structure stored at room temperature for two months, and found that its mechanical properties were similar to those of the newly manufactured microneedle structure. It can still return to its original shape under repeated pressing. We have added a video of microneedle for repeated compressions in the ESI†(see ESI Video S1).

3.4 The electrical conductivity of functional materials

Fig. 7 shows the conductivity of the polymer corresponding to the increase of the content of MXene from 0.2 wt% to 3 wt%. With the MXene content of 3 wt%, the conductivity of the polymer can reach 0.0035 S m^{-1}. With the Mxene content of 0.2 wt%, the conductivity of the polymer can still reach 0.0025 S m^{-1}. However, when the concentration of MXene increases from 0.2 wt% to 0.5 wt%, there is a downward trend in the conductivity of the polymer. This may be caused by the uneven dispersal of MXene into the polymer with 0.5 wt% of MXene. The above experimental results show that among the polymers containing 0.2 wt% Mxene, the conductive material Mxene has the best dispersion in the polymer. And despite the fact that there are fewer conductive materials, a good conductive network can still be constructed.

3.5 Biocompatibility of 3D scaffolds

In this study, we verified the biocompatibility of the polymer structure by live-dead cell experiments. We cultured human lung epithelial cells on the polymer grid structure prepared by four kinds of materials respectively. Fig. 8a and b show the results of DAPI staining of BEAS-2B cells cultured for 24 hours and 72 hours respectively. From the results shown in the Fig. 8, it can be found that the cell viability is close to 100%. After 72 hours of culture, the cell density increased significantly compared to the density after 24 hours of culture, indicating that the material is not cytotoxic and the polymer mesh structure can support the proliferation of BEAS-2B cells. A small amount of red image in the dead part in Fig. 8 is due to the normal apoptosis of cells and the residue of red dye that has not been cleaned.

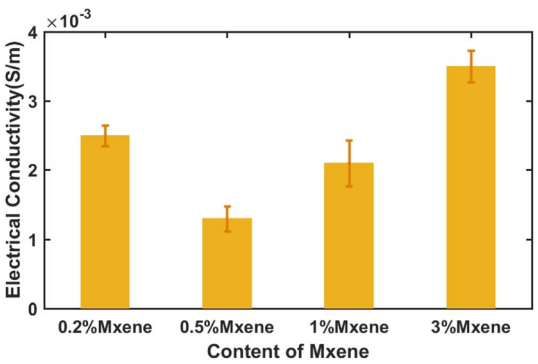

Fig. 7 Electrical conductivity of polymer corresponding to different concentrations of MXene.

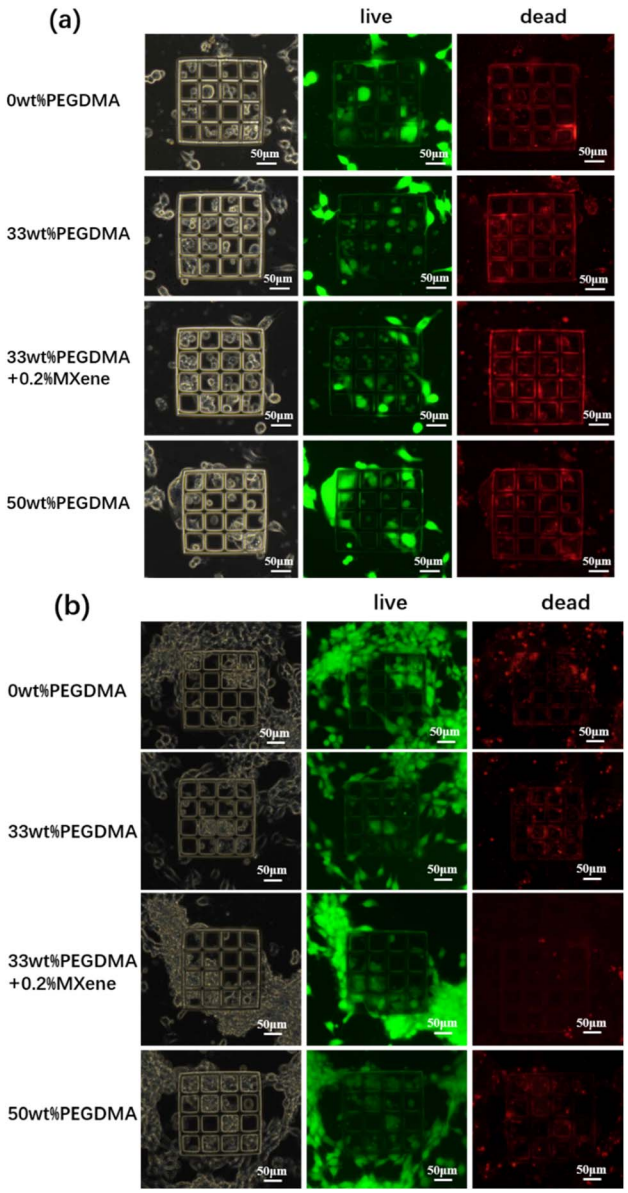

Fig. 8 (a) Live-dead assay of BEAS-2B cells cultured on scaffold surface for 24 h. (b) Live-dead assay of BEAS-2B cells cultured on scaffold surface for 72 h.

4. Conclusions

This study proposes a biocompatible photoresist formulation with tunable mechanical properties and doped MXene conductive material. First of all, this research focuses on the resolution of materials. By studying the structure of nanowires, we found that when the laser scanning speed remains constant, the smaller the laser intensity, the higher the printing resolution; when the laser intensity is constant, the greater the laser speed, the higher the printing resolution. Subsequently, this study used the above-mentioned photoresist materials to prepare scaffold structures, high-aspect-ratio microneedle structures, Shanghai University micro-logo and micro-helical robot structures, which further verified that our proposed

photoresist materials have high stability and excellent printability. At the same time, the Young's modulus of the polymer structure can be adjusted between 0.3 GPa and 1.5 GPa by changing the ratio of PEG600DMA. Next, for photoresist materials with conductivity, this study achieved a doping amount of MXene up to 0.2 wt%, and obtained a conductivity of 0.0025 S m^{-1}. Finally, human normal lung epithelial cells (BEAS-2B) were cultured on the 2D structure for 1–3 days to carry out or dead cell experiments, and the results fully showed that the polymer structure we prepared had good biocompatibility. And, we believe that our new material can be applied to living tissue engineering,[32,33] cell engineering[7] and micro–nano robot.[34,35]

Author contributions

Lijun Men conceived the project and carried out most of the writing and performed the main experimental work and analyzed the data. Kemin Wang, Ningning Hu, Fule Wang and Yucheng Deng, helped with the experimental work and data analysis. Ruixue Yin and Chris Zhang helped with the topic guidance, experimental design, data analysis and article revision. All authors contributed to writing and editing the manuscript.

Conflicts of interest

There are no conflicts to declare.

Acknowledgements

We would like to thank Mingche Biotechnology (Suzhou) Co., Ltd. for financial support and technical support. At the same time, we would also like to thank Anton Paar for mechanical tests.

Notes and references

1 J.-F. Xing, M.-L. Zheng and X.-M. Duan, *Chem. Soc. Rev.*, 2015, **44**, 5031–5039.
2 A. K. Nguyen and R. J. Narayan, *Mater. Today*, 2017, **20**, 314–322.
3 C. Liao, A. Wuethrich and M. Trau, *Appl. Mater. Today*, 2020, **19**, 100635.
4 M. Carlotti and V. Mattoli, *Small*, 2019, **15**, 1902687.
5 W. Xiong, Y. Liu, L.-J. Jiang, Y.-S. Zhou, D.-W. Li, L. Jiang, J. F. Silvain and Y.-F. Lu, *Adv. Mater.*, 2016, **28**, 2002–2009.
6 X. Zhou, Y. Hou and J. Lin, *AIP Adv.*, 2015, **5**, 030701.
7 H. Yu, J. Liu, Y.-Y. Zhao, F. Jin, X.-Z. Dong, Z.-S. Zhao, X.-M. Duan and M.-L. Zheng, *Adv. Healthcare Mater.*, 2019, **2**, 3077–3083.
8 R. Wollhofen, M. Axmann, P. Freudenthaler, C. Gabriel, C. Rohrl, H. Stangl, T. A. Klar and J. Jacak, *ACS Appl. Mater. Interfaces*, 2018, **10**, 1474–1479.
9 M. R. Gullo, S. Takeuchi and O. Paul, *ACS Appl. Bio Mater.*, 2017, **6**, 1601053.
10 A. Accardo, M.-C. Blatché, R. Courson, I. Loubinoux, C. Thibault, L. Malaquin and C. Vieu, *Small*, 2017, **13**, 1700621.
11 K. Arcaute, B. Mann and R. Wicker, *Acta Biomater.*, 2010, **6**, 1047–1054.
12 L. Brigo, A. Urciuolo, S. Giulitti, G. Della Giustina, M. Tromayer, R. Liska, N. Elvassore and G. Brusatin, *Acta Biomater.*, 2017, **55**, 373–384.
13 H. Ceylan, I. C. Yasa, O. Yasa, A. F. Tabak, J. Giltinan and M. Sitti, *ACS Nano*, 2019, **13**, 3353–3362.
14 S. D. Gittard, P. R. Miller, R. D. Boehm, A. Ovsianikov, B. N. Chichkov, J. Heiser, J. Gordon, N. A. Monteiro-Riviere and R. J. Narayan, *Faraday Discuss.*, 2011, **149**, 171–185.
15 J. Jiang, H. S. Gill, D. Ghate, B. E. McCarey, S. R. Patel, H. F. Edelhauser and M. R. Prausnitz, *Invest. Ophthalmol. Visual Sci.*, 2007, **48**, 4038–4043.
16 J. Jiang, J. S. Moore, H. F. Edelhauser and M. R. Prausnitz, *Pharm. Res.*, 2009, **26**, 395–403.
17 C.-M. Ho, S. H. Ng, K. H. Li and Y.-J. Yoon, *Lab Chip*, 2015, **15**, 3627–3637.
18 E. K. Sackmann, A. L. Fulton and D. J. Beebe, *Nature*, 2014, **507**, 181–189.
19 K. Venkatakrishnan, S. Jariwala and B. Tan, *OSA*, 2009, **17**, 2756–2762.
20 D. Jang, J. Jeong, H. Song and S. K. Chung, *J. Micromech. Microeng.*, 2019, **29**, 053002.
21 S. Mohanty, J. Zhang, J. M. McNeill, T. Kuenen, F. P. Linde, J. Rouwkema and S. Misra, *Sens. Actuators, B*, 2021, **347**, 130589.
22 T. Wei, J. Liu, D. Li, S. Chen, Y. Zhang, J. Li, L. Fan, Z. Guan, C.-M. Lo, L. Wang, K. Man and D. Sun, *Small*, 2020, **16**, e1906908.
23 J. Li and M. Pumera, *Chem. Soc. Rev.*, 2021, **50**, 2794–2838.
24 S. Kim, F. Qiu, S. Kim, A. Ghanbari, C. Moon, L. Zhang, B. J. Nelson and H. Choi, *Adv. Mater.*, 2013, **25**, 5863–5868.
25 D. Wu, S.-Z. Wu, L.-G. Niu, Q.-D. Chen, R. Wang, J.-F. Song, H.-H. Fang and H.-B. Sun, *Appl. Phys. Lett.*, 2010, **97**, 031109.
26 E. Avci, M. Grammatikopoulou and G. Z. Yang, *Adv. Opt. Mater.*, 2017, **5**, 1700031.
27 S. Tottori, L. Zhang, F. Qiu, K.-K. Krawczyk, A. Franco-Obregón and B. J. Nelson, *Adv. Mater.*, 2012, **24**, 811–816.
28 T.-Y. Huang, M. S. Sakar, A. Mao, A. J. Petruska, F. Qiu, X.-B. Chen, S. Kennedy, D. Mooney and B. J. Nelson, *Adv. Mater.*, 2015, **27**, 6644–6650.
29 H. Rastin, B. Zhang, A. Mazinani, K. Hassan, J. Bi, T. T. Tung and D. Losic, *Nanoscale*, 2020, **12**, 16069.
30 J. Xing, L. Liu, X. Song, Y. Zhao, L. Zhang, X. Dong, F. Jin, M. Zheng and X. Duan, *J. Mater. Chem. B*, 2015, **3**, 8486–8491.
31 B. Buchroithner, D. Hartmann, S. Mayr, Y. J. Oh, D. Sivun, A. Karner, B. Buchegger, T. Griesser, P. Hinterdorfer, T. A. Klar and J. Jacak, *Nanoscale Adv.*, 2020, **2**, 2422–2428.
32 J. Maciulaitis, S. Rekštytė, M. Bratchikov, R. Gudas, M. Malinauskas, A. Pockevicius, A. Usas, A. Rimkunas, V. Jankauskaite, V. Grigaliunas and R. Maciulaitis, *Appl. Surf. Sci.*, 2019, **487**, 692–702.

33 H. N. Kim, A. Jiao, N. S. Hwang, M. S. Kim, D. H. Kang, D.-H. Kim and K. Y. Suh, *Adv. Drug Delivery Rev.*, 2013, **65**, 536–558.
34 X.-Z. Chen, M. Hoop, N. Shamsudhin, T. Huang, B. Ozkale, Q. Li, E. Siringil, F. Mushtaq, L. Di Tizio, B. J. Nelson and S. Pane, *Adv. Mater.*, 2017, **29**, 8.
35 M. Suter, L. Zhang, E. C. Siringil, C. Peters, T. Luehmann, O. Ergeneman, K. E. Peyer, B. J. Nelson and C. Hierold, *Biomed. Microdevices*, 2013, **15**, 997–1003.